Fabrication of Self-Cleaning, Reusable Titania Templates for Nanometer and Micrometer Scale Protein Patterning

Mark Moxey,[†,‡] Alexander Johnson,[†] Osama El-Zubir,[†] Michael Cartron,[§] Saman Safari Dinachali,[‡] C. Neil Hunter,[§] Mohammad S. M. Saifullah,[‡] Karen S. L. Chong,[*,‡] and Graham J. Leggett[*,†]

[†]Department of Chemistry, University of Sheffield, Sheffield S3 7HF, United Kingdom, [‡]Institute of Materials Research and Engineering (IMRE), A*STAR (Agency for Science, Technology and Research), 3 Research Link, Singapore 117602, Republic of Singapore, and [§]Department of Molecular Biology and Biotechnology, University of Sheffield, Western Bank, Sheffield S10 2TN, United Kingdom

ABSTRACT The photocatalytic self-cleaning characteristics of titania facilitate the fabrication of reuseable templates for protein nanopatterning. Titania nanostructures were fabricated over square centimeter areas by interferometric lithography (IL) and nanoimprint lithography (NIL). With the use of a Lloyd's mirror two-beam interferometer, self-assembled monolayers of alkylphosphonates adsorbed on the native oxide of a Ti film were patterned by photocatalytic nanolithography. In regions exposed to a maximum in the interferogram, the monolayer was removed by photocatalytic oxidation. In regions exposed to an intensity minimum, the monolayer remained intact. After exposure, the sample was etched in piranha solution to yield Ti nanostructures with widths as small as 30 nm. NIL was performed by using a silicon stamp to imprint a spin-cast film of titanium dioxide resin; after calcination and reactive ion etching, TiO_2 nanopillars were formed. For both fabrication techniques, subsequent adsorption of an oligo(ethylene glycol) functionalized trichlorosilane yielded an entirely passive, protein-resistant surface. Near-UV exposure caused removal of this protein-resistant film from the titania regions by photocatalytic degradation, leaving the passivating silane film intact on the silicon dioxide regions. Proteins labeled with fluorescent dyes were adsorbed to the titanium dioxide regions, yielding nanopatterns with bright fluorescence. Subsequent near-UV irradiation of the samples removed the protein from the titanium dioxide nanostructures by photocatalytic degradation facilitating the adsorption of a different protein. The process was repeated multiple times. These simple methods appear to yield durable, reuseable samples that may be of value to laboratories that require nanostructured biological interfaces but do not have access to the infrastructure required for nanofabrication.

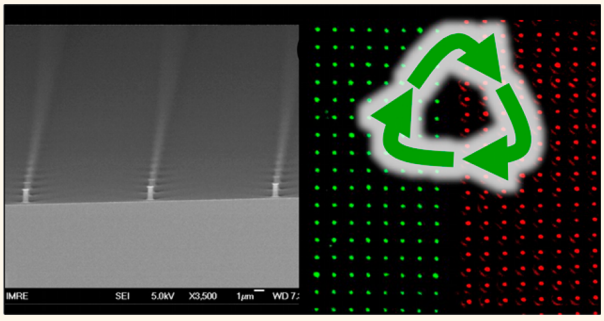

KEYWORDS: nanofabrication · photolithography · nanoimprint lithography · interferometric lithography · titania · photocatalysis · protein arrays

The organization of proteins at surfaces is necessary for applications in array-based biosensor technology,[1−4] and for fundamental work that aims to examine the relationship between the spatial organization of biological molecules and diverse phenomena including tissue cell attachment,[5−8] actin filament formation,[9] neuronal guidance, membrane protein function, biological recognition and energy transfer in light-harvesting complexes.[10,11] There has been a great deal of interest in the development of techniques for the organization of proteins on nanometer length scales, but to date, there have been few reports of methods that provide control over protein organization on sub-100 nm length scales. Protein patterning is highly challenging because proteins adsorb strongly and irreversibly to most surfaces; rigorous control of nonspecific adsorption is required simultaneously with the definition of protein-binding regions. Examples to date include the use of microcontact printing,[12] colloidal self-assembly, dip-pen nanolithography,[13,14] nanoshaving,[15] electron-beam lithography[16,17] and near-field optical techniques.[18−20] However, local probe and electron-beam techniques are serial in nature and thus not well suited to large area fabrication. Moreover, samples fabricated in this way are "single-use" materials that cannot be reused with a different biological

* Address correspondence to karen-chong@imre.a-star.edu.sg, Graham.Leggett@sheffield.ac.uk.

Received for review March 16, 2015 and accepted June 4, 2015.

Published online June 04, 2015
10.1021/acsnano.5b01636

adsorbate. Recently, interferometric lithography (IL) has been used to fabricate protein nanopatterns over macroscopic (cm^2) areas by photochemical degradation of novel protein-resistant poly(cysteine methacrylate) brushes[21] and by degradation of protein-resistant silanes,[22] with a feature size of 30 nm reported in the latter case. Such methods are attractive because they enable rapid, inexpensive fabrication of macroscopically extended arrays of nanostructured biomolecules, but they are still subject to the limitation that fresh substrates must be fabricated for each experiment.

The photocatalytic properties of titania are well-documented.[23−25] Irradiation by photons with energies larger than the band gap leads to the formation of electron−hole pairs, with the consequence that excited oxygen species are formed, leading to the oxidative degradation of organic matter at the surface. Photocatalytic degradation processes have been used to pattern organic resist layers including films of siloxanes,[26] alkylphosphonates,[27−31] alkylthiolates[27] and graphene.[32] Gradient structures have been fabricated, by using a grayscale mask to carry out exposure,[27] and combination of photocatalysis with a local probe has enabled nanofabrication to be attempted.[33] Recently, a titania-coated AFM probe was used to write 70 nm protein structures in a protein-resistant silane film,[34] by exploiting the photocatalytic properties of the oxide film to cause localized degradation of a protein-resistant silane film, rendering it adhesive.

For laboratories that are interested in the organization of proteins on nanometer length scales, but do not possess extensive infrastructure for nanofabrication, the availability of reuseable templates for protein adsorption, in which features are formed with high fidelity over large areas (*ca.* 0.1−1.0 cm^2), would be highly attractive. In this work, we demonstrate that titania nanostructures, formed by either interferometric lithography (IL)[35] of a self-assembled monolayer (SAM) of alkylphosphonates[36−42] or by nanoimprint lithography (NIL) of a novel titania resin, may be utilized in combination with the adsorption of protein-resistant silanes to produce nanometer-scale protein patterns (Figure 1). The photocatalytic properties of the titania templates mean that they may be cleaned by UV exposure, and degradation products simply rinsed away prior to reuse for adsorption of a different protein.

RESULTS AND DISCUSSION

Photolithographic Fabrication of Micro- and Nanostructures. Micrometer- and nanometer-scale titanium structures were fabricated as shown in Figure 1a by photocatalytic patterning of an alkylphosphonates SAM as resist. Exposure through a mask caused photocatalytic degradation of the monolayer in exposed regions, while the monolayer remained intact in masked regions. To

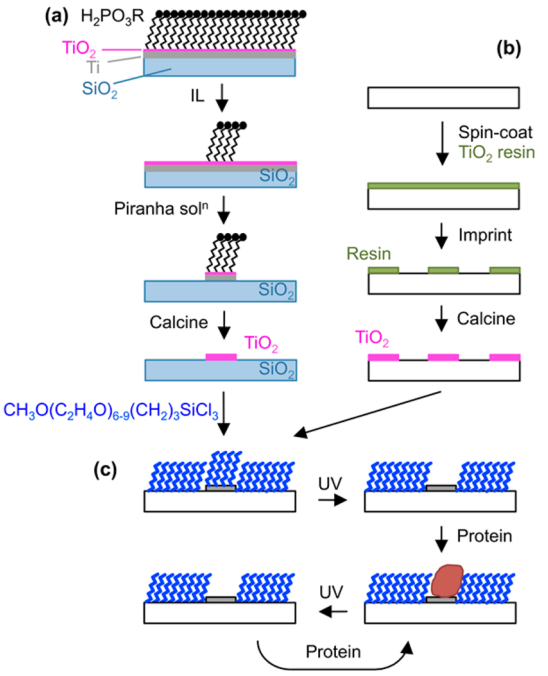

Figure 1. Schematic diagram showing the fabrication and functionalization of titanium dioxide nanostructures. (a) Photocatalytic nanopatterning of an alkylphosphonate self-assembled monolayer on titanium dioxide, by exposure to UV light in a Lloyd's mirror interferometer or through a mask, leads to selective removal of the adsorbates facilitating selective etching of the titanium dioxide film using piranha solution. (b) Nanoimprint lithography of a resin layer formed by spin-coating TiO_2 resin containing mixture of monomers onto a silicon wafer, followed by calcination, yields TiO_2 nanostructures. (c) Arrays of titania nanostructures fabricated by both approaches are coated by adsorption of an oligo(ethylene glycol) functionalized trichlorosilanes, rendering them protein-resistant. Exposure of the samples to near-UV light causes photocatalytic cleaning of titania regions, facilitating protein adsorption. Further cycles of near-UV exposure and protein adsorption may be carried out, enabling multiple reuse of samples.

create nanostructures, light from a frequency-doubled argon ion laser (244 nm) was directed into a Lloyd's mirror interferometer consisting of a sample and mirror set at an angle 2θ to each other; half the incident beam was directed onto the sample, and the other half was reflected from the mirror onto the sample, where it interfered with the first half of the beam to yield a pattern of alternating bands of constructive and destructive interference, with period $\lambda/2 \sin \theta$. In regions where the sample was exposed to a maximum of intensity, the adsorbates were photocatalytically degraded, but in areas exposed to a minimum in the interferogram, modification was limited. Consequently, when the samples were etched, using piranha solution, the titanium was removed from regions exposed to a maximum in the interferogram, but in regions where the sample was exposed to a band of destructive interference, the SAM remained intact and thus masked the titanium from the etch solution.

Figure 2 shows Ti nanostructures fabricated in this fashion. The period and full width at half-maximum

height (fwhm) of the Ti nanostructures may be varied by changing the angle 2θ between the two interfering beams in the interferometer and by varying the etch time. In Figure 2a, structures with a fwhm of 250 nm have been formed at a 900 nm period, while in Figure 2b, structures with a fwhm of 30 nm have been formed at a 150 nm period. To facilitate efficient photocatalysis in subsequent protein patterning work, titanium dioxide was annealed by heating to 550 °C. It was found that annealed samples yielded higher rates of photocatalytic degradation than the as-prepared films, an observation that was attributed to the formation of the photocatalytically active anatase phase. While the titania surface used in the initial lithographic step was likely a mixture of anatase and rutile, it proved straightforward to pattern the SAMs because of the high energy of the photons (244 nm). After annealing, the titanium structures became resistant to etching in piranha solution; it was thus important that calcination was carried out after the nanofabrication process had been completed, and not beforehand.

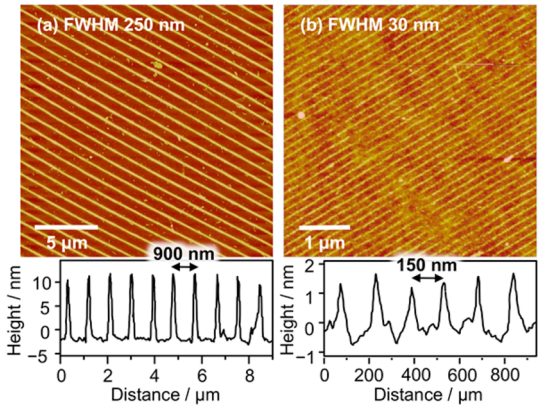

Figure 2. Tapping mode (a) and contact mode (b) AFM height images, together with representative line sections, of titanium nanowires formed by interferometric lithography. Exposure of an octadecylphosphonate SAM on the native oxide layer of a thin film of titanium was followed by etching in piranha solution.

TiO_2 micro- or nanostructures were immersed in a solution of [methoxy(polyethyleneoxy)propyl]-trichlorosilane ($CH_3O(C_2H_4O)_{6-9}$ $(CH_2)_3Cl_3Si$, henceforth OEG-silane) in toluene, to form a film of protein-resistant silane across the entire surface. Ellipsometry indicated a thickness of *ca.* 2 nm, similar to the expected thickness of a monolayer of adsorbate, although the thickness of the film is likely variable and ellipsometry alone cannot provide confirmation of monolayer formation. The sample was then exposed to UV light from the HeCd laser (325 nm), causing photocatalytic degradation of the OEG-silane molecules attached to the titania surface and rendering those regions adhesive to proteins.

The modification of the silane film was characterized by using X-ray photoelectron spectroscopy to analyze unpatterned films of OEG-silane formed on titanium and silicon oxide surfaces (Figure 3). The as-prepared films on both substrates yield a strong ether component in the C 1s spectrum at 286.7 eV, together with a second component at 285.0 eV that corresponds to hydrocarbon. After exposure of the film on titanium dioxide to a UV dose of 1.53 J cm^{-2} at 325 nm, the ether peak was observed to be significantly reduced, and new peaks were observed at 287.8 and 289.1 eV corresponding to aldehyde and carboxylic acid products of the photocatalytic degradation process. In contrast, the C 1s spectra of the films formed by adsorption of OEG-silane on silicon dioxide surfaces showed no signs of change even after an exposure as high as 48 J cm^{-2} (Figure 3e).

After selective removal of OEG-silane from Ti microstructures, the samples were immersed in a solution of FITC-labeled immunoglobulin G (FITC-IgG) in

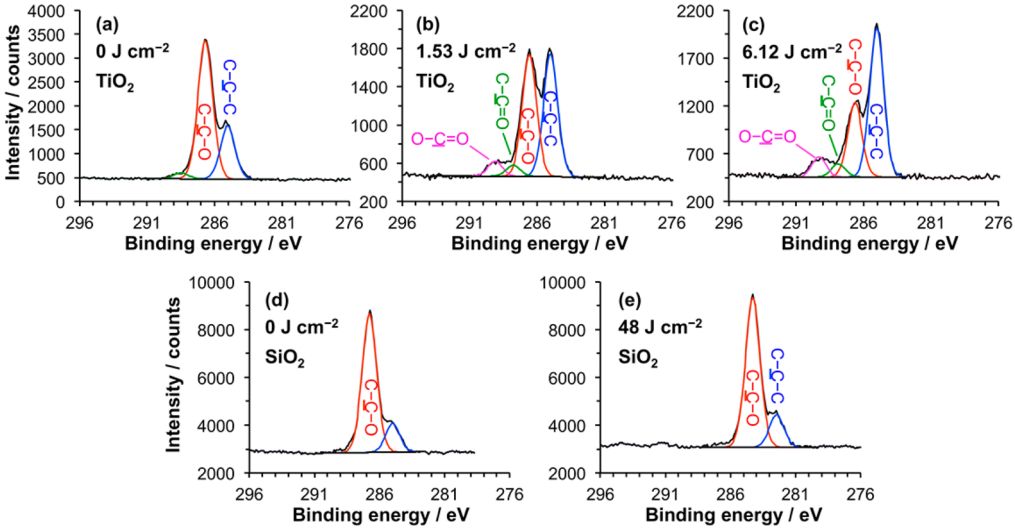

Figure 3. XPS C 1s spectra for films of OEG-silane formed on titanium dioxide (a–c) and silicon dioxide (d and e) after various UV exposures at a wavelength of 325 nm.

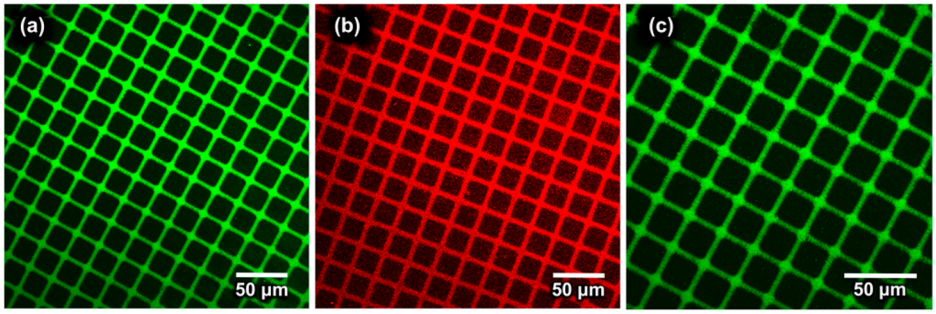

Figure 4. Confocal fluorescence microscopy images of Ti microstructures following repeated cycles of photocatalytic cleaning and adsorption of (a) FITC-IgG, (b) Cy3-streptavidin, and (c) FITC-IgG.

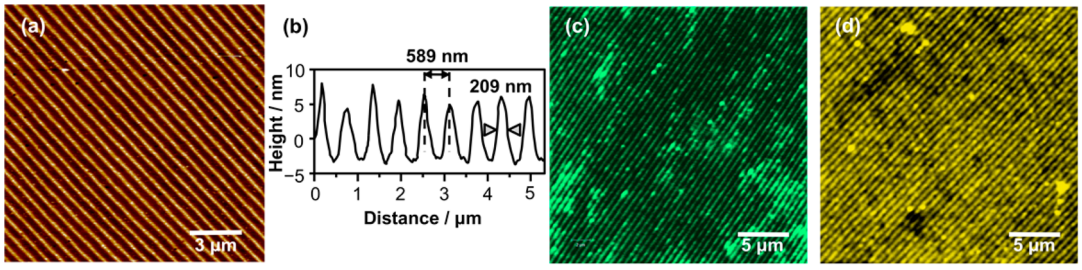

Figure 5. (a) Tapping mode AFM height image of TiO_2 nanostructures fabricated for protein nanopatterning experiments. (b) Line section showing a period of 589 nm and fwhm of 209 nm. (c) Confocal fluorescence micrograph after adsorption of GFP onto the sample shown in (a). (d) Fluorescence micrograph of the sample shown in (c) after photocatalytic cleaning of the TiO_2 nanostructures followed by adsorption of YFP.

phosphate-buffered saline (PBS) solution. Protein adsorbed to titanium dioxide coated regions in which the surface was not protected by OEG-silane. The sample was imaged by confocal fluorescence microscopy (Figure 4a). Bright green fluorescence may be observed from the TiO_2 regions (bars), but the square regions, which consist of OEG-silane-coated silicon dioxide, remain dark because the oligo(ethylene glycol) groups are highly protein resistant and remained intact in those regions.

A further exposure was carried out using the HeCd laser, to cause photocatalytic degradation of protein attached to titania. The sample was immersed in a solution of Cy3-labeled streptavidin, and imaged by confocal fluorescence microscopy (Figure 4b). Bright fluorescence was observed at 543 nm from the TiO_2 regions (bars), but the OEG-silane functionalized silicon dioxide regions (squares) remained dark, confirming that the streptavidin had adsorbed only to the titania surface. Finally, the sample was cleaned by exposure at 325 nm, leading to photocatalytic breakdown of the streptavidin, and the surface was refunctionalized by adsorption of FITC-IgG (Figure 4c).

Protein nanopatterns were formed on structures fabricated by interferometric lithography. To enable the resulting patterns to be resolved by confocal fluorescence microscopy, a period of 589 nm was selected, larger than the point spread function of the imaging system. For these samples (Figure 5a), a fwhm of 209 nm was measured. Given that some broadening of the features is expected in the micrographs, these dimensions are close to the lower limit that is feasible if protein adsorption is to be detected by fluorescence microscopy. After adsorption of green fluorescent protein (GFP), clear bands of green fluorescence were observed from the TiO_2 structures (Figure 5c). The protein bands, while broadened because of the intrinsic limitations of the imaging system, could clearly be resolved from the dark regions between the TiO_2 nanostructures that were passivated with OEG-silane. The sample was photocatalytically cleaned, by exposure to light from the HeCd laser, and immersed in a solution of yellow fluorescent protein (YFP). The YFP adsorbed to the clean surfaces of the TiO_2 nanostructures, and again, the protein nanolines could be resolved from the dark, OEG-passivated lines separating them (Figure 5d). These data demonstrate that TiO_2 nanostructures may be utilized to fabricate protein nanopatterns, yielding excellent contrast in fluorescence microscopy. They also demonstrate that such structures may be reused by exploiting the photocatalytic self-cleaning characteristics of titanium dioxide, with no loss of protein-resistance in neighboring silicon dioxide regions that have been passivated with OEG-silane.

After exposure to the HeCd laser, both micrometer- and nanometer-scale titania patterns appeared completely dark in confocal microscopy images. In an effort to quantify the removal of protein in the photocatalytic step, a simple control experiment was performed using an unpatterned film that had been treated in all other respects in the same way as the patterned samples

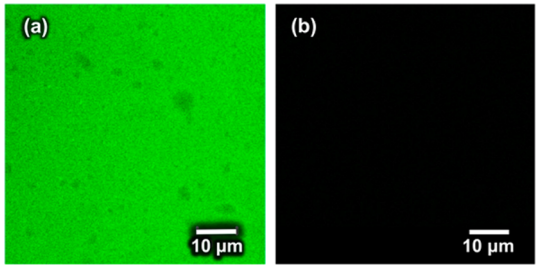

Figure 6. Confocal fluorescence micrographs of an unpatterned control sample, onto which a monolayer of GFP has been adsorbed, before (a) and after (b) photocatalytic cleaning. The mean grayscale intensity of each pixel was 64.7 AU in (a) and 2.2 AU in (b).

were. Because of the small size of the nanostructures, and the comparatively low levels of fluorescence detected even when they were coated with protein, a macroscopic control specimen was judged to be a more accurate means by which to determine the efficiency of photocatalytic cleaning. Figure 6 shows fluorescence images acquired under identical gain conditions for a specimen before and after exposure to UV light. The mean fluorescence intensity at each pixel was determined. Before exposure, the mean intensity was 64.7 arbitrary units (AU); after exposure, it was 2.2 AU. In our microscope, the background signal is never exactly zero, and the intensity after UV exposure, which was *ca.* 3% of the intensity beforehand, likely reflects the background noise level in the fluorescence experiment, supporting the qualitative observation that protein fluorescence was undetectable after photocatalytic cleaning.

Fabrication of Protein Nanostructures by Nanoimprint Lithography. Titania nanostructures were also fabricated by nanoimprint lithography. IL and NIL are somewhat different fabrication methods, and our goal was to determine whether titania nanofabrication provided a generically useful approach to the fabrication of reusable templates for protein patterning. While NIL requires more sophisticated infrastructure than IL, it is not restricted to the fabrication of periodic structures, as is the case for IL, offering greater freedom in the design of nanostructures.

Titanium dioxide pillars were fabricated using NIL. The process is shown schematically in Figure 1b. TiO_2 resin was spin-coated onto a glass substrate, and the film was patterned by NIL. Figure 7a shows a cross-sectional image acquired by scanning electron microscopy (SEM) for a representative sample. The resulting structures were calcined to remove the organic components in the imprinted film, which resulted in a 60−70% shrinkage in the dimensions of the structures (Figure 7b). A thin residual film remained between the nanostructures. It was difficult to resolve by SEM, but if left intact, yielded a continuous thin film of titania between the nanostructures defined by NIL. The residual layer was removed by reactive ion etching (RIE) in

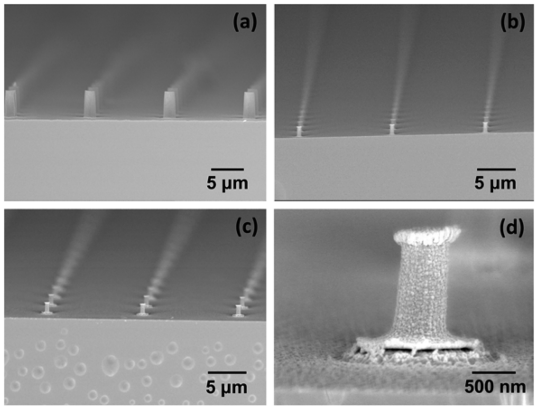

Figure 7. SEM cross-sectional images of (a) an array of imprinted TiO_2 resin pillars; (b) a similar structure after calcination at 550 °C; (c) the finished TiO_2 structure after reactive ion etching with SF_6 and Ar gases; and (d) a high magnification image showing complete removal of the TiO_2 residual layer.

an SF_6 and Ar gas mixture. Figure 7c shows the finished structures. A high magnification image of a single pillar is shown in Figure 7d. This micrograph shows clearly the interface between the TiO_2 pillar and the SiO_2 below and surrounding it. A clear interface to the TiO_2 may be seen, confirming that it is an isolated structure.

After fabrication of the array of TiO_2 pillars, OEG-silane was adsorbed onto the entire sample, creating a protein-resistant layer. The sample was flooded with near-UV radiation, causing photocatalytic degradation of OEG-silane molecules on the TiO_2 pillars. Protein patterns were prepared by immersing the sample in a solution of fluorescein-conjugated wheat germ agglutinin (FITC-WGA). Figure 8 shows confocal fluorescence microscopy images of FITC-WGA adsorbed onto three different TiO_2 structures fabricated by NIL. In Figure 8, panels a and b show arrays of TiO_2 dots with diameters of 600 and 200 nm, respectively, and periods of 12 and 1 μm, respectively. Figure 8c shows an array of TiO_2 lines with a width of *ca.* 250 nm and a period of 5 μm. In each case, the TiO_2 nanostructures exhibit bright fluorescence, and the oxide regions between them, wich have been passivated using OEG-silane, exhibit dark contrast, suggesting that nonspecific adsorption of proteins is negligible. These data confirm the effectiveness of using TiO_2 nanofabrication, combined with the photocatalytic properties of the titanium dioxide surface, to control protein adsorption.

Samples were subjected to repeated cycles of protein adsorption and photocatalytic cleaning. Figure 9 shows data for a sample that consisted of 200 nm TiO_2 dots at a period of 1000 nm. The sample was treated with OEG-silane, to render it protein-resistant, and then exposed to UV light to remove the silane from the TiO_2 dots by photocatalytic degradation. The sample was then immersed in a solution of Cy5-labeled streptavidin (henceforth Cy5−streptavidin) in buffer overnight and then rinsed and imaged by confocal fluorescence

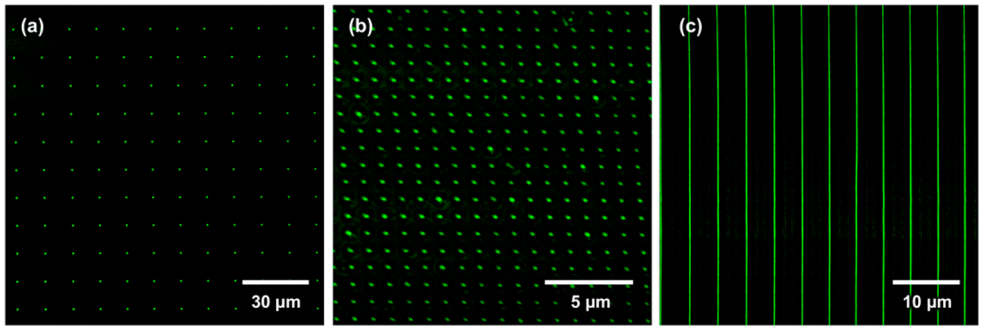

Figure 8. Confocal fluorescence microscopy images showing FITC-WGA adsorbed to TiO_2 patterns consisting of (a) 0.6 μm dots, (b) 0.2 μm dots, and (c) 0.25 μm lines.

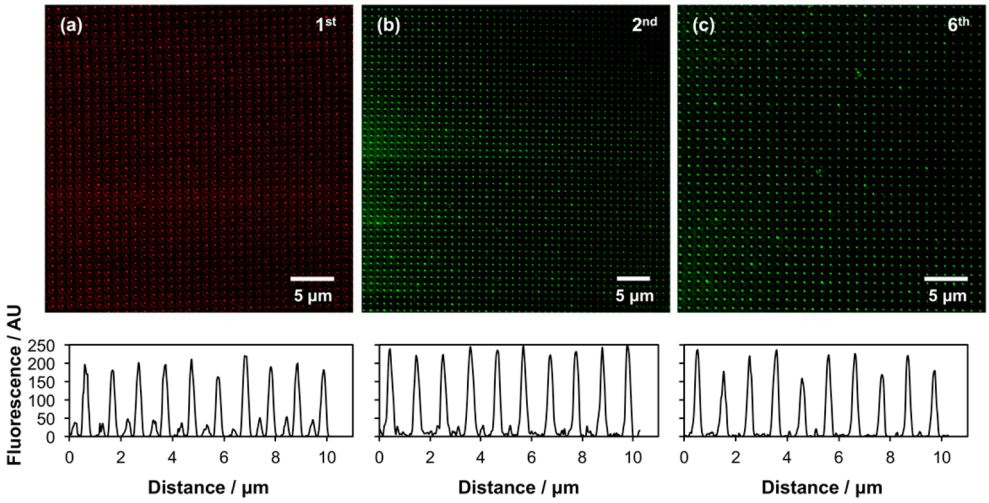

Figure 9. Confocal fluorescence microscopy images of a single 0.2 μm TiO_2 dot array sample following repeated cycles of protein adsorption and photocatalytic cleaning. (a) Image acquired after the first cycle, showing Cy5−streptavidin adsorbed onto an array of TiO_2; (b) image acquired after a second cycle, showing ITC-WGA adsorbed to titania pillars following photocatalytic cleaning of the sample shown in (a); (c) image acquired after a sixth cycle showing FITC-WGA adsorbed to titania pillars following consecutive adsorption and removal of FITC-WGA and Cy5−streptavidin proteins.

microscopy (Figure 9a). The Cy5−streptavidin coated TiO_2 nanodots are resolved clearly. The surrounding OEG-silane passivated regions are dark, confirming that they remained protein-resistant. The cross section through the fluorescence image exhibits negligible fluorescence from these regions.

The sample was cleaned by exposure to UV light, and immersed in a solution of FITC-WGA in buffer. The sample was rinsed and imaged by confocal fluorescence microscopy (Figure 9b). Strong fluorescence is observed from the TiO_2 nanodots, and again, the cross section through the fluorescence micrograph shows that the fluorescence intensity from the OEG-silane regions between the dots remains negligible.

The process was repeated further times. The sample was, on each occasion, cleaned by exposure to UV light and then immersed in solutions of Cy5−streptavidin (odd numbered cycles) and FITC-WGA (even numbered cycles). Figure 9c shows a fluorescence image of the sample after the sixth cycle. Despite repeated cycles of protein adsorption and photocatalytic cleaning, the fluorescence remains negligible on the regions between the TiO_2 nanodots, confirming that the OEG-silane is resilient under near-UV exposure, and the fluorescence on the nanodots remains bright, confirming that the protein-adhesive surface is successfully regenerated by UV exposure.

CONCLUSIONS

The photocatalytic self-cleaning characteristics of titania surfaces provide a simple means to fabricate reuseable templates for protein nanopatterning. Titanium nanostructures may be fabricated by interferometric lithography, using a simple dual-beam Lloyd's mirror interferometer to pattern a self-assembled monolayer of alkylphosphonates on the native oxide layer of a Ti thin film by photocatalytic degradation. The modified surface is etched with piranha solution to yield Ti nanostructures with full widths at half-maximum as small as 30 nm. Alternatively, nanoimprint lithography may be used to pattern a spin-cast film of titanium dioxide resin that was subsequently calcined and treated by reactive ion etching to remove residual layer from between the

imprinted structures. In both cases, the silicon oxide regions between the TiO_2 structures may be passivated with an oligo(ethylene glycol) terminated silane, rendering them resistant to protein adsorption. In both cases, protein can be selectively adsorbed to the TiO_2 nanostructures, and subsequently removed by exposure to near-UV radiation, with negligible degradation of the passivating silane film between the TiO_2 nanostructures. This facilitates multiple reuse of the TiO_2 structures as templates for protein nanopatterning.

METHODS

SAM Preparation. Glass coverslips (Menzel-Glaser, 22 mm × 60 mm, no. 2 thickness) and silicon (100) wafers (Pi-Kem, Tamworth, U.K.) were initially cleaned with fuming piranha solution, which is a mixture of 30% H_2O_2 and 98% concentration sulfuric acid (both purchased from Fisher scientific) in the ratio 3:7 for 40 min. (*Caution!*: *Piranha solution is a strong oxidizing agent, which has been known to detonate spontaneously upon contact with organic material, and should be handled with extreme care.*) The substrates were rinsed excessively with deionized water and dried in an oven at 120 °C overnight. Titanium dioxide substrates were prepared by evaporating a 15−20 nm of titanium onto the glass slides at a rate of 0.03 nm s^{-1} using an Edwards Auto306 vacuum coating system. The evaporator was allowed to cool before venting to dry nitrogen. To allow the formation of the native oxide layer, the slides were exposed to the laboratory atmosphere for 20 min. SAMs were formed on the titanium dioxide substrate by immersing them in a solution of 1 mM octadecylphosphonic acid (Alfa Aesar, Heysham, U.K., 97%) in toluene for 12−48 h. Following the formation of the SAM, the samples were rinsed with toluene and ethanol and dried under a stream of nitrogen.

Micropatterning. SAMs of ODPA on titanium were exposed in air to light from a frequency-doubled argon ion laser emitting at 244 nm (Coherent FreD 300C). The laser power was measured at 33.7 mW cm^{-2}. Patterns were produced by exposing the sample through a Cu TEM grid. The photopatterned samples were immersed in cold piranha solution and kept at 30 °C using a water bath for approximately 25 min. The end point of the etching was roughly determined by eye and then later confirmed by AFM, ensuring the height of the titanium features were similar to the initial evaporated thickness. After etching, the samples were rinsed thoroughly with deionized water and ethanol. The samples were calcined at 550 °C for 1 h.

SAMs of OEG-silane were formed on the etched samples by placing them in a 1 mM solution of 2-[methoxy(polyethyleneoxy)-propyl]-trichlorosilane (OEG-silane, Fluorochem, Hadfield, U.K.) in toluene for 2 h. To remove the OEG-silane from the titanium dioxide, the samples were exposed to a 325 nm UV laser (Kimmon model IK3202R-D, HeCd) at a dose of 8.65 J cm^{-2} and then rinsed with ethanol and water. Protein adsorption was carried out by immersing the samples in 10 μL mL^{-1} of Streptavidin−Cy3 or IgG-FITC, pH 7.4, 10 mM phosphate buffered saline solution overnight. The samples were rinsed with deionized water and then dried under a stream of nitrogen before imaging with confocal microscopy. Subsequent removal of the protein was achieved by irradiating the sample at 325 nm wavelengths with a dose of 14.4 J cm^{-2}.

IL. Interference lithography was carried out using a Lloyd's mirror interferometer in conjunction with the frequency-doubled argon ion laser. The angle between the mirror and the sample in the interferometer was varied depending on the period of the pattern required. Samples were patterned using the IL with a dose of between 1.68 and 3.93 J cm^{-1}. Following photopatterning, the samples were rinsed with ethanol and the titanium substrates were etched by placing in warm piranha solution (40 °C) for 4−6 min. The samples were then rinsed with deionized water and calcined in an oven at 550 °C for 1 h.

SAMs of OEG-silane were formed on the etched samples by placing them in a 1 mM solution of OEG-silane in toluene for 2 h. To remove the OEG-silane from titania, the samples were exposed to the HeCd laser at a dose of 8.65 J cm^{-2} and then rinsed with ethanol and water. Protein adsorption was carried out by immersing the samples in 20 μg mL^{-1} of GFP or YFP in pH 7.4, 100 mM ammonium acetate buffer solution overnight. The samples were rinsed with deionized water and then dried under a stream of nitrogen before imaging with confocal microscopy.

NIL. Titanium(IV) *n*-butoxide (97%), 2-(methacryloyloxy) ethyl acetoacetate (95%) and ethylene glycol dimethacrylate (98%) were purchased from Sigma-Aldrich and used as received. Benzoyl peroxide (BPO) was supplied by Sinopharm Chemical Reagent. 2-[Methoxy(polyethyleneoxy)propyl]-trichlorosilane (OEG-silane) was supplied by Fluorochem. Absolute ethanol (99.8+%) was supplied by Fisher Scientific.

All glassware and silicon wafers used were first cleaned by submersion in piranha solution, a mixture of 30% hydrogen peroxide and 95% concentrated sulfuric acid in the ratio 3:7 for at least 40 min. (*Caution!: Piranha solution is an extremely strong oxidizing agent which has been known to detonate spontaneously upon contact with organic material.*) The glassware was rinsed thoroughly with deionized water (Elgar Nanopure, 18.2 MΩ) a minimum of six times and then sonicated for 10 min before being placed in the oven (approximately 80 °C) and left overnight to dry.

A titanium dioxide resin was made by combining titanium-(IV) *n* -butoxide with 2-(methacryloyloxy) ethyl acetoacetate in 1:2 molar ratio inside a glovebox (<5% relative humidity) to form the chelated precursor with an alcohol as by product. Then, ethylene glycol dimethacrylate as a cross-linker was added to the chelated precursor followed by benzoyl peroxide (BPO), an initiator for thermal free radical polymerization.[43]

The titanium dioxide resin was spin-coated onto glass substrates at 3000 rpm for 30 s. The monomer film was imprinted with silicon molds using an Eitre 6 (Obducat) nanoimprinting system. Samples were imprinted at 35 bar, and for the first 300 s, the temperature was set at 30 °C, then the temperature was raised to 135 °C and the samples cured for 600 s before the pressure was released and the mold removed. After the imprinting step, the samples were calcined in an oven at 550 °C for 1 h. The residual layer was removed by an RIE process using a Plasmalab 80 Plus (Oxford Instruments). The pressure and power were set at 80 mTorr and 125 W, respectively. SF_6 and Ar gas were supplied at flow rates of 30 and 10 sccm, respectively, for an etch time of 1 min. The samples were then cleaned with fuming piranha solution and rinsed with ultrapure DI water. SAMs of OEG-silane were formed on the etched samples by placing them in a 1 mM solution of OEG-silane in toluene for 2 h. The samples were then irradiated by a UV-A lamp emitting wavelengths in the range 320 −400 nm for 3 min to remove the OEG-silane molecules bound to the TiO_2 structures. Protein adsorption was carried out by immersing the samples overnight in 10 μL mL^{-1} of streptavidin−Cy5 or wheat germ agglutinin-fluorescein (WGA-FITC), pH 7.4, 10 mM phosphate buffered saline solution. The samples were rinsed with deionized water and then dried under a stream of nitrogen before imaging with confocal microscopy. Subsequent removal of the protein was achieved analogous to the removal of the PEG-silane, by irradiating the sample with a UV-A lamp for 3 min.

Preparation of GFP and YFP. The gene sequence of yellow fluorescent protein (YFP) was amplified by PCR from pCS2-Venus vector (a kind gift from Dr. Atsushi Miyawaki, RIKEN Brain Science Institute, Japan). The resulting Nde I /BamHI fragment was cloned into a pET14b expression vector (Novagen). Introducing the combined F64L, S65T, V68L, S72A, M153T, V163A, S175G, A206 K mutations into the YFP gene resulted in enhanced green fluorescent protein (GFP) gene.[44] Both His_6-YFP

and His_6-GFP proteins were produced by heterologous expression in *Escherichia coli* (BL21); cells were grown to an OD_{680} of 0.6 at 37 °C, then induced using IPTG (0.4 mM) for 12 h at 25 °C. Pelleted cells (19 000*g*/20 min) were lysed by sonication and the resulting lysate was clarified by a further spin (33 000*g*/30 min). Both His-tagged fluorescent proteins were purified to homogeneity from clarified lysate using a Chelating Sepharose Fast Flow Ni-NTA gravity flow column (GE Healthcare) as detailed in the manufacturer's instructions. Protein purity was assessed by gel electrophoresis (SDS−PAGE).

Characterization. XPS measurements were made using a Kratos Axis Ultra X-ray photoelectron spectrometer, equipped with a delay-line detector and operating at a base pressure of 1×10^{-9} mbar. Survey spectra were acquired at pass energy of 160 eV, and high resolution spectra at pass energy of 20 eV. All XPS spectra were analyzed and curve-fitted using the Casa XPS software, and were corrected relative to the C 1s signal at binding energy (B.E.) = 285.0 eV.

Tapping AFM measurements were made using a Bruker Nanoscope IV Multimode atomic force microscope. RTESP probes with a nominal tip radius 8 nm and TESP-SS series ultrasharp silicon probes (Bruker), with resonance frequency of 320−350 kHz and an average tip radius of 2 nm, were used.

Fluorescence images were acquired with a LSM 510 Meta laser scanning confocal microscope (Carl Zeiss, Welwyn Garden City, U.K.). The samples were mounted in a glycerol/PBS-based antifade solution (Citifluor AF1, Agar Scientific, U.K.) and observed with 40× and 63× oil immersion objectives (numerical apertures of 1.30 and 1.40, respectively). A small drop of immersion oil (Immersol 518 F, Zeiss) was placed on the slide in the center of the lighted area. All fluorescence images were analyzed using Zeiss LSM image browser software.

Conflict of Interest: The authors declare no competing financial interest.

Acknowledgment. The authors thank EPSRC (Grant EP/I012060/1) for a Programme Grant. M.M. thanks the A*STAR-Sheffield Research Attachment Program (ARAP) for a research studentship and also the A*STAR Nanoimprint Foundry (IMRE/13-2B0278) for project funding. C.N.H. gratefully acknowledges financial support from the Biotechnology and Biological Sciences Research Council (BBSRC U.K.), award number BB/G021546/1. C.N.H. was also supported by an Advanced Award 338895 from the European Research Council and as part of the Photosynthetic Antenna Research Center (PARC), an Energy Frontier Research Center funded by the U.S. Department of Energy, Office of Science, Office of Basic Energy Sciences under Award Number DE-SC 0001035. PARC's role was to provide partial support for C.N.H.

REFERENCES AND NOTES

1. Lee, S.-W.; Lee, K.-S.; Ahn, J.; Lee, J.-J.; Kim, M.-G.; Shin, Y.-B. Highly Sensitive Biosensing Using Arrays of Plasmonic Au Nanodisks Realized by Nanoimprint Lithography. *ACS Nano* **2011**, *5*, 897–904.
2. Canalejas-Tejero, V.; Herranz, S.; Bellingham, A.; Moreno-Bondi, M. C.; Barrios, C. A. Passivated Aluminum Nanohole Arrays for Label-Free Biosensing Applications. *ACS Appl. Mater. Interfaces* **2013**, *6*, 1005–1010.
3. Turner, A. P. F. Biosensors: Sense and Sensibility. *Chem. Soc. Rev.* **2013**, *42*, 3184–3196.
4. Ahijado-Guzmán, R.; Prasad, J.; Rosman, C.; Henkel, A.; Tome, L.; Schneider, D.; Rivas, G.; Sönnichsen, C. Plasmonic Nanosensors for Simultaneous Quantification of Multiple Protein−Protein Binding Affinities. *Nano Lett.* **2014**, *14*, 5528–5532.
5. Lopez, G. P.; Albers, M. W.; Schreiber, S. L.; Carroll, R.; Peralta, E.; Whitesides, G. M. Convenient Methods for Patterning the Adhesion of Mammalian Cells to Surfaces using Self-Assembled Monolayers of Alkanethiolates on Gold. *J. Am. Chem. Soc.* **1993**, *115*, 5877–5978.
6. Singhvi, R.; Kumar, A.; Lopez, G. P.; Stephanopoulos, G. N.; Wang, D. I. C.; Whitesides, G. M.; Ingber, D. E. Engineering Cell Shape and Function. *Science* **1994**, *264*, 696–698.
7. Chen, C. S.; Mrksich, M.; Huang, S.; Whitesides, G. M.; Ingber, D. E. Geometric control of cell life and death. *Science* **1997**, *276*, 1425–1428.
8. Lee, K.-B.; Park, S.-J.; Mirkin, C. A.; Smith, J. C.; Mrksich, M. Nanoarrays Generated by Dip-Pen Nanolithography. *Science* **2002**, *295*, 1702–1705.
9. Cavalcanti-Adam, E. A.; Volberg, T.; Micoulet, A.; Kessler, H.; Geiger, B.; Spatz, J. P. Cell Spreading and Focal Adhesion Dynamics Are Regulated by Spacing of Integrin Ligands. *Biophys. J.* **2007**, *92*, 2964–2974.
10. Reynolds, N. P.; Janusz, S. J.; Escalante-Marun, M.; Timney, J.; Ducker, R. E.; Olsen, J. D.; Otto, C.; Subramanian, V.; Leggett, G. J.; Hunter, C. N. Directed Formation of Micro- and Nanoscale Patterns of Functional Light Harvesting LH2 Complexes. *J. Am. Chem. Soc.* **2007**, *129*, 14625–14631.
11. Escalante, M.; Lenferink, A.; Zhao, Y.; Tas, N.; Huskens, J.; Hunter, C. N.; Subramaniam, V.; Otto, C. Long-Range Energy Propagation in Nanometer Arrays of Light Harvesting Antenna Complexes. *Nano Lett.* **2010**, *10*, 1450–1450.
12. Coyer, S. R.; García, A. J.; Delamarche, E. Facile Preparation of Complex Protein Architectures with Sub-100-nm Resolution on Surfaces. *Angew. Chem., Int. Ed.* **2007**, *46*, 6837–684.
13. Piner, R. D.; Zhu, J.; Xu, F.; Hong, S.; Mirkin, C. A. "Dip-Pen" Nanolithography. *Science* **1999**, *283*, 661–663.
14. Lim, J.-H.; Ginger, D. S.; Lee, K.-B.; Heo, J.; Nam, J.-M.; Mirkin, C. A. Direct-Write Dip-Pen Nanolithography of Proteins on Modified Silicon Oxide surfaces. *Angew. Chem., Int. Ed.* **2003**, *42*, 2309–2312.
15. Zhou, D.; Wang, X.; Birch, L.; Rayment, T.; Abell, C. AFM Study on Protein Immobilization on Charged Surfaces at the Nanoscale: Toward the Fabrication of Three-Dimensional Protein Nanostructures. *Langmuir* **2003**, *19*, 10557–10562.
16. Ballav, N.; Thomas, H.; Winkler, T.; Terfort, A.; Zharnikov, M. Making Protein Patterns by Writing in a Protein-Repelling Matrix. *Angew. Chem., Int. Ed.* **2009**, *48*, 5833–5836.
17. Krakert, S.; Ballav, N.; Zharnikov, M.; Terfort, A. Adjustment of the Bioresistivity by Electron Irradiation: Self-Assembled Monolayers of Oligo(ethyleneglycol)-Terminated Alkanethiols with Embedded Cleavable Group. *Phys. Chem. Chem. Phys.* **2010**, *12*, 507–515.
18. Montague, M.; Ducker, R. E.; Chong, K. S. L.; Manning, R. J.; Rutten, F. J. M.; Davies, M. C.; Leggett, G. J. Fabrication of Biomolecular Nanostructures by Scanning Near-Field Photolithography of Oligo(ethylene glycol) Terminated Self-Assembled Monolayers. *Langmuir* **2007**, *23*, 7328–7337.
19. Reynolds, N. P.; Tucker, J. D.; Davison, P. A.; Timney, J. A.; Hunter, C. N.; Leggett, G. J. Site-Specific Immobilization and Micrometer and Nanometer Scale Photopatterning of Yellow Fluorescent Protein on Glass Surfaces. *J. Am. Chem. Soc.* **2009**, *131*, 896–897.
20. Alang Ahmad, S. A.; Wong, L. S.; ul-Haq, E.; Hobbs, J. K.; Leggett, G. J.; Micklefield, J. Protein Micro- and Nanopatterning Using Aminosilanes with Protein-Resistant Photolabile Protecting Groups. *J. Am. Chem. Soc.* **2011**, *133*, 2749–2759.
21. Alswieleh, A. M.; Cheng, N.; Canton, I.; Ustbas, B.; Xue, X.; Ladmiral, V.; Xia, S.; Ducker, R. E.; El Zubir, O.; Cartron, M. L.; et al. Zwitterionic Poly(amino acid methacrylate) Brushes. *J. Am. Chem. Soc.* **2014**, *136*, 9404–9413.
22. Tizazu, G.; el Zubir, O.; Patole, S.; McLaren, A.; Vasilev, C.; Mothersole, D.; Adawi, A.; Hunter, C. N.; Lidzey, D.; Lopez, G.; et al. Micrometer and Nanometer Scale Photopatterning of Proteins on Glass Surfaces by Photo-Degradation of Films Formed from Oligo(ethylene glycol) Terminated Silanes. *Biointerphases* **2012**, *7*, 1–9.
23. Wang, R.; Hashimoto, K.; Fujishima, A.; Chikuni, M.; Kojima, E.; Kitamura, A.; Shimohigoshi, M.; Watanabe, T. Light-Induced Amphiphilic Surfaces. *Nature* **1997**, *388*, 431–432.
24. Haick, H.; Paz, Y. Remote Photocatalytic Activity As Probed by Measuring the Degradation of Self-Assembled Monolayers Anchored near Microdomains of Titanium Dioxide. *J. Phys. Chem. B* **2001**, *105*, 3045–3054.
25. Haick, H.; Paz, Y. "Dark" Photocatalysis: The Degradation of Organic Molecules Anchored to Dark Microdomains of Titanium Dioxide. *ChemPhysChem* **2003**, *4*, 617–620.

26. Lee, J. P.; Kim, H. K.; Park, C. R.; Park, G.; Kwak, H. T.; Koo, S. M.; Sung, M. M. Photocatalytic Decomposition of Alkylsiloxane Self-Assembled Monolayers on Titanium Oxide Surfaces. *J. Phys. Chem. B* **2003**, *107*, 8997–9002.
27. Blondiaux, N.; Zurcher, S.; Liley, M.; Spencer, N. D. Fabrication of Multiscale Surface-Chemical Gradients by Means of Photocatalytic Lithography. *Langmuir* **2007**, *23*, 3489–3494.
28. Soja, G. R.; Watson, D. F. TiO2-Catalyzed Photodegradation of Porphyrins: Mechanistic Studies and Application in Monolayer Photolithography. *Langmuir* **2009**, *25*, 5398–5403.
29. Tizazu, G.; Adawi, A.; Leggett, G. J.; Lidzey, D. G. Photopatterning, Etching, and Derivatization of Self-Assembled Monolayers of Phosphonic Acids on the Native Oxide of Titanium. *Langmuir* **2009**, *25*, 10746–10753.
30. Nakata, K.; Nishimoto, S.; Yuda, Y.; Ochiai, T.; Murakami, T.; Fujishima, A. Rewritable Superhydrophilic-Superhydrophobic Patterns on a Sintered Titanium Dioxide Substrate. *Langmuir* **2010**, *26*, 11628–11630.
31. Paz, Y. Self-assembled monolayers and titanium dioxide: From surface patterning to potential applications. *Beilstein J. Nanotechnol.* **2011**, *2*, 845–861.
32. Zhang, L.; Diao, S.; Nie, Y.; Yan, K.; Liu, N.; Dai, B.; Xie, Q.; Reina, A.; Kong, J.; Liu, Z. Photocatalytic Patterning and Modification of Graphene. *J. Am. Chem. Soc.* **2011**, *133*, 2706–2713.
33. Kobayashi, K.; Tomita, Y.; Maeda, Y. Nanolithography Based on Photocatalysis of TiO_2 Using an Atomic Force Microscope. *Jpn. J. Appl. Phys.* **2005**, *44*, 5829–583.
34. Ul-Haq, E.; Patole, S.; Moxey, M.; Amstad, E.; Vasilev, C.; Hunter, C. N.; Leggett, G. J.; Spencer, N. D.; Williams, N. H. Photocatalytic Nanolithography of Self-Assembled Monolayers and Proteins. *ACS Nano* **2013**, *7*, 7610–761810.
35. Brueck, S. R. J. Optical and Interferometric Lithography—Nanotechnology Enablers. *Proc. IEEE* **2005**, *93*, 1704–172.
36. Textor, M.; Ruiz, L.; Hofer, R.; Rossi, A.; Feldman, K.; Hahner, G.; Spencer, N. D. Structural Chemistry of Self-Assembled Monolayers of Octadecylphosphonic Acid on Tantalum Oxide Surfaces. *Langmuir* **2000**, *16*, 3257–3271.
37. Tosatti, S.; Michel, R.; Textor, M.; Spencer, N. D. Self-Assembled Monolayers of Dodecyl and Hydroxy-dodecyl Phosphates on Both Smooth and Rough Titanium and Titanium Oxide Surfaces. *Langmuir* **2002**, *18*, 3537–3548.
38. Zwahlen, M.; Tosatti, S.; Textor, M.; Hahner, G. Orientation in Methyl- and Hydroxyl-Terminated Self-Assembled Alkanephosphate Monolayers on Titanium Oxide Surfaces Investigated with Soft X-Ray Absorption. *Langmuir* **2002**, *18*, 3957–3962.
39. Spori, D. M.; Venkataraman, N. V.; Tosatti, S. G. P.; Durmaz, F.; Spencer, N. D.; Zurcher, S. Influence of Alkyl Chain Length on Phosphate Self-Assembled Monolayers. *Langmuir* **2007**, *23*, 8053–8060.
40. Ramsier, R. D.; Henriksen, P. N.; G, A. N. Adsorption of Phosphorus Acids on Alumina. *Surf. Sci.* **1988**, *203*, 72–88.
41. Gao, W.; Dickinson, L.; Grozinger, C.; Morin, F. G.; Reven, L. Self-Assembled Monolayers of Alkylphosphonic Acids on Metal Oxides. *Langmuir* **1996**, *12*, 6429–6435.
42. Cao, G.; Hong, H.-G.; Mallouk, T. E. Layered Metal Phosphates and Phosphonates: From Crystals to Monolayers. *Acc. Chem. Res.* **1992**, *25*, 420–427.
43. Dinachali, S. S.; Saifullah, M. S. M.; Ganesan, R.; Thian, E. S.; He, C. A Universal Scheme for Patterning of Oxides *via* Thermal Nanoimprint Lithography. *Adv. Funct. Mater.* **2013**, *23*, 2201–2211.
44. Kramers, G. J.; Goedhart, J.; van Munster, E. B.; Gadella, T. W. J. Cyan and Yellow Super Fluorescent Proteins with Improved Brightness, Protein Folding, and FRET Förster Radius. *Biochemistry* **2006**, *45*, 6570–6580.